BIOCHEMISTRY
including biophysical chemistry & molecular biology

Article

pubs.acs.org/biochemistry

# Membrane Docking of the Synaptotagmin 7 C2A Domain: Electron Paramagnetic Resonance Measurements Show Contributions from Two Membrane Binding Loops

J. Ryan Osterberg, Nara Lee Chon, Arthur Boo, Favinn A. Maynard, Hai Lin, and Jefferson D. Knight*

Department of Chemistry, University of Colorado Denver, Denver, Colorado 80217, United States

Supporting Information

**ABSTRACT:** The synaptotagmin (Syt) family of proteins plays an important role in vesicle docking and fusion during $Ca^{2+}$-induced exocytosis in a wide variety of cell types. Its role as a $Ca^{2+}$ sensor derives primarily from its two C2 domains, C2A and C2B, which insert into anionic lipid membranes upon binding $Ca^{2+}$. Syt isoforms 1 and 7 differ significantly in their $Ca^{2+}$ sensitivity; the C2A domain from Syt7 binds $Ca^{2+}$ and membranes much more tightly than the C2A domain from Syt1, at least in part because of greater contributions from the hydrophobic effect. While the structure and membrane activity of Syt1 have been extensively studied, the structural origins of differences between Syt1 and Syt7 are unknown. This study used site-directed spin labeling and electron paramagnetic resonance spectroscopy to determine depth parameters for the Syt7 C2A domain, for comparison to analogous previous measurements with the Syt1 C2A domain. In a novel approach, the membrane docking geometry of both Syt1 and Syt7 C2A was modeled by mapping depth parameters onto multiple molecular dynamics-simulated structures of the $Ca^{2+}$-bound protein. The models reveal membrane penetration of $Ca^{2+}$ binding loops 1 (CBL1) and 3 (CBL3), and membrane binding is more sensitive to mutations in CBL3. On average, Syt7 C2A inserts more deeply into the membrane than Syt1 C2A, although depths vary among the different structural models. This observation provides a partial structural explanation for the hydrophobically driven membrane docking of Syt7 C2A.

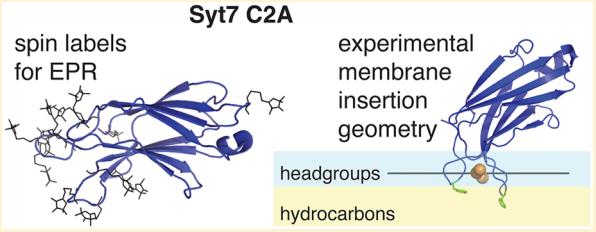


Synaptotagmins (Syt) make up a family of proteins characterized by their membrane-targeting C2 domains. Syt proteins contain a transmembrane helix that anchors a cytoplasmic region consisting of two C2 domains (C2A and C2B) connected by a short linker.[1,2] Each C2 domain is composed of two four-stranded $\beta$-sheets forming a $\beta$-sandwich structure with three flexible $Ca^{2+}$ binding loops, although not all Syt C2 domains bind $Ca^{2+}$.[3,4] There are 17 human isoforms of Syt, eight of which show varying degrees of $Ca^{2+}$ binding affinity.[5−7] The individual C2 domains of each Syt exhibit a variety of affinities; for example, Syt1 C2A binds anionic lipids such as phosphatidylserine (PS) nonspecifically in the presence of $Ca^{2+}$, while Syt1 C2B additionally binds phosphatidylinositol 4,5-bisphosphate ($PIP_2$) in a partially $Ca^{2+}$-independent fashion.[8−12] Syt1 C2B additionally interacts with the soluble *N*-ethylmaleimide-sensitive fusion protein attachment receptor (SNARE) protein SNAP25 in a manner proposed to inhibit vesicle fusion prior to $Ca^{2+}$ influx.[13−15] Influx of $Ca^{2+}$ into the cytoplasm releases the fusion clamp and triggers membrane insertion by the two Syt C2 domains, thereby accelerating vesicle fusion.[1,6,14] The mechanism by which this happens is unknown but believed to rely on the membrane insertion and bending activity of Syt; mutations that disrupt C2 domain membrane interactions also decrease the level of exocytosis.[16−19] Thus, a better understanding of the structural mechanism of Syt C2 domain membrane binding is central to a fuller description of exocytosis.

Much of what is currently known about the structure of membrane-bound Syt comes from studies using electron paramagnetic resonance (EPR) spectroscopy. EPR detects the relaxation of unpaired electrons excited by incident microwaves within a magnetic field of 8−10 GHz. Incorporation of unpaired electrons into a protein of interest involves an established approach known as site-directed spin labeling,[20] in which unique cysteine residues are introduced at locations of interest in the target protein through site-directed mutagenesis. A nitroxide spin label such as MTSSL is then attached through formation of a disulfide bond to the engineered cysteine. EPR spectra are useful for observing local environmental interactions with the unpaired nitroxide electron, and an application termed continuous wave power saturation is capable of measuring protein−membrane docking geometry.[21,22] Power saturation relies on the accessibility of a spin label to various paramagnetic probes. The EPR signal amplitude increases linearly with the square root of the incident power up to a saturation point, which is dependent on the relaxation rate of the spin label. Heisenberg spin exchange between the spin label and extrinsic paramagnetic probes increases the relaxation rate; thus, power saturation measurements reveal the relative accessibility of the spin label to each paramagnetic probe. Paramagnetic probes

**Received:** April 18, 2015
**Revised:** August 30, 2015
**Published:** August 31, 2015





DOI: 10.1021/acs.biochem.5b00421
*Biochemistry* 2015, 54, 5684−5695

with differing concentration gradients in a membrane such as $O_2$ (predominantly in the membrane interior) and nickel ethylenediaminediacetic acid (NiEDDA, excluded from the membrane) allow for the calculation of membrane depth parameters (Φ). The depth parameters from a library of spin-labeled protein variants can be mapped onto a known structure of the protein to calculate an optimized membrane docking geometry to fit the experimental results.[21]

To date, the most extensively studied member of the Syt family is Syt1, which acts as a $Ca^{2+}$ sensor for the fast synchronous release of synaptic vesicles in neuronal cells. This is the fastest known membrane fusion event, occurring on the microsecond to millisecond time scale.[1,23,24] Previous EPR power saturation studies have revealed the membrane docking geometries of Syt1 C2A and C2B, both individually and in the context of the C2AB tandem.[25−27] In agreement with qualitative studies based on fluorescence changes,[28,29] these EPR measurements demonstrated that both Syt1 C2A and C2B insert more deeply into membranes in the context of the C2AB tandem.[30] The precise mechanism by which C2A−C2B copenetration occurs is unknown. Interestingly, EPR experiments utilizing double electron−electron resonance (DEER) distance measurements of Syt1 C2AB fragments have yielded models requiring the CBLs of C2A and C2B to be oriented in opposite directions when membrane-bound, consistent with this protein's observed ability to induce negative curvature in membranes.[31] By contrast, the isolated Syt1 C2A domain binds membranes via a combination of electrostatic and hydrophobic interactions, dominated by electrostatic contacts within the polar headgroup region.[25,32,33] Its docking geometry shows membrane penetration by CBL1 and CBL3, with CBL1 located entirely within the headgroup region and CBL3 inserting somewhat more deeply.[25] Each of these loops contains a single hydrophobic residue at its apex: M173 on loop 1 and F234 on loop 3 of Syt1. Intriguingly, while F234 is conserved among all stimulatory Syt isoforms, M173 is somewhat variable, for example, corresponding to Phe in Syt7 and Ser in Syt3.[6,7] It is not yet known whether the membrane binding properties of Syt1 are common to other Syt isoforms.

Presumably, the variability among Syt isoforms is indicative of the various and complex functions this family of proteins has evolved to fill.[34] Syt7, although not as well studied as Syt1, performs many important functions. In particular, Syt7 is involved in the regulation of insulin secretion in pancreatic β-cells. Dysregulation of insulin secretion has been implicated in the development of type 2 diabetes, and in part, efforts to further understand the underlying factors of this disease have led to research into the structure and function of this protein.[35,36] Similar to Syt1 C2A, Syt7 C2A binds nonspecifically to anionic lipid headgroups with no particular affinity for $PIP_2$ beyond simple electrostatic interactions.[37] The Syt7 C2A domain, however, is sensitive to much lower concentrations of $Ca^{2+}$ and also exhibits a membrane dissociation rate 60-fold slower than that of Syt1 C2A.[37,38] We have previously shown that the slower off rate of Syt7 C2A can be attributed in part to a stronger hydrophobic component of the Syt7 C2A docking mechanism, and we hypothesized that this is mainly due to deeper membrane penetration by F167 on CBL1.[37]

Here, we test our previous hypothesis by measuring the docking geometry of the Syt7 C2A domain using methods analogous to those previously used for Syt1 C2A. We report depth parameters for 13 separate spin-labeled mutants, including key locations in CBL1 and CBL3. These data are interpreted by modeling docking geometry based on these depth parameters and five protein structures: three from a molecular dynamics simulation of $Ca^{2+}$-bound Syt7 C2A, and two for comparison from a publically accessible $Ca^{2+}$-free solution nuclear magnetic resonance (NMR) structure. The results suggest a somewhat deeper membrane penetration for the isolated Syt7 C2A than for Syt1 C2A, anchored primarily via CBL3 and secondarily by CBL1. The following paper in this issue (DOI: 10.1021/acs.biochem.5b00422) describes molecular dynamics simulations of Syt7 C2A binding to a lipid bilayer, revealing a balance between hydrophobic and electrostatic effects.

## EXPERIMENTAL PROCEDURES

**Materials.** All materials were reagent grade unless otherwise specified. Synthetic lipids 1-palmitoyl-2-oleoyl-*sn*-glycero-3-phosphocholine (phosphatidylcholine, POPC, or PC) and 1-palmitoyl-2-oleoyl-*sn*-glycero-3-phosphoserine (phosphatidylserine, POPS, or PS) were obtained from Avanti Polar Lipids (Alabaster, AL) in chloroform. The spin label 1-oxyl-2,2,5,5-tetramethyl-$\Delta^3$-pyrroline-3-methylmethanethiosulfonate (MTSSL or R1) was from Toronto Research Chemicals. Fluorescein 5-maleimide was from AnaSpec (Fremont, CA). Doxyl lipids 1-palmitoyl-2-stearoyl(12-doxyl)-*sn*-glycero-3-phosphocholine (12-doxyl PC), 1-palmitoyl-2-stearoyl(10-doxyl)-*sn*-glycero-3-phosphocholine (10-doxyl PC), 1-palmitoyl-2-stearoyl(7-doxyl)-*sn*-glycero-3-phosphocholine (7-doxyl PC), and 1-palmitoyl-2-stearoyl(5-doxyl)-*sn*-glycero-3-phosphocholine (5-doxyl PC) were from Avanti Polar Lipids. *N*-[5-(Dimethylamino)naphthalene-1-sulfonyl]-1,2-dihexadecanoyl-*sn*-glycero-3-phosphoethanolamine (dansyl-PE or dPE) was from Life Technologies.

**Protein Mutagenesis, Expression, Spin Labeling, and Purification.** The initial goal for protein mutagenesis was to create a cysteine-free (cysless) variant of Syt7 C2A, so that unique cysteine residues could be introduced at desired positions. A GST-fused C2A expression construct encompassing residues N135−S266 was cloned from cDNA (ATCC catalog no. 11045721) as previously described.[37] Mutations were generated using the QuikChange II XL (Agilent) site-directed mutagenesis kit using the manufacturer's protocol. The cysless mutant of Syt7 C2A, C260S, was used as the parent DNA for developing a library of single-cysteine mutants. A total of 17 single-cysteine mutants were created at the positions listed in Table 1. All mutations were verified by primer extension sequencing of the full C2A coding sequence.

Each single mutant was expressed as a fusion protein with a GST tag and purified via a glutathione affinity resin (GE Healthcare) as previously described, including elution with assay buffer [140 mM KCl, 25 mM HEPES, 15 mM NaCl, and 0.5 mM $MgCl_2$ (pH 7.4)] following thrombin cleavage between the GST and C2A domains.[37] Labeling with the methanethiosulfonate spin label (MTSSL) was achieved by incubating protein with MTSSL either for 1 h at 4 °C while the GST-C2A fusion protein was bound to the resin or overnight at 4 °C following thrombin cleavage and elution, with approximately equivalent labeling efficiencies of >75% obtained in either case (Figure S1). Protein purity was verified by SDS−PAGE and ultraviolet absorbance spectroscopy. Because of the positive charge on Syt 7 C2A, contamination with nucleic acids is sometimes observed and can interfere with protein−lipid binding.[39] Thus, high-salt washes were included in the column purification protocol. We note that this removal was more


DOI: 10.1021/acs.biochem.5b00421
*Biochemistry* 2015, 54, 5684−5695

**Table 1. Measured Rate Constants for Kinetic Measurements**

| species | $k_{off}$ ($s^{-1}$)[a] | $k_{off}$ relative to C260S | $k_{obs}$ for binding ($s^{-1}$)[b] | $k_{obs}$ relative to C260S |
|---|---|---|---|---|
| wild type | 26 | 1.5 | 27 | 0.47 |
| C260S (cysless) | 17 | 1 | 57 | 1 |
| L136R1 | 19 | 1.1 | 35 | 0.61 |
| Q148R1 | 20 | 1.2 | 27 | 0.47 |
| A164R1[c] | 21 | 1.2 | 18 | 0.32 |
| F167R1 | 27 | 1.6 | 52 | 0.91 |
| S168R1 | 34 | 2.0 | 29 | 0.51 |
| G169R1 | 19 | 1.1 | 25 | 0.44 |
| T170R1 | 19 | 1.1 | 51 | 0.89 |
| N195R1 | 33 | 1.9 | 65 | 1.14 |
| L196R1 | 38 | 2.2 | 60 | 1.05 |
| L224R1 | 35 | 2.1 | 34 | 0.60 |
| Y226R1[c] | 69 | 4.1 | 5 | 0.09 |
| R228R1 | 24 | 1.4 | 73 | 1.28 |
| F229R1[c] | 69 | 4.1 | 34 | 0.60 |
| R231R1 | 16 | 0.9 | 50 | 0.88 |
| N232R1 | 23 | 1.4 | 34 | 0.60 |
| P234R1 | 21 | 1.2 | 65 | 1.14 |

[a]Measured by rapid addition of excess EDTA to a preformed protein−$Ca^{2+}$−liposome complex. [b]Measured by rapidly mixing protein and liposomes in the presence of excess $Ca^{2+}$. [c]Species excluded from further study because of aberrant kinetics.

critical for kinetic measurements of protein−membrane association than for EPR measurements. Samples with an $OD_{260}/OD_{280}$ ratio of ≤1.0, indicating only minor levels of contamination, were determined to be acceptable. Any purified proteins showing a ratio of >1.0 were further treated with benzonase (Sigma) for 1 h at 25 °C, and a new spectrum was recorded to confirm the removal of nucleic acid. EPR measurements are less sensitive to nucleic acid contamination because of the large excess of lipid vesicles and the long time period over which measurements are taken, allowing protein-membrane binding to reach equilibrium. Concentrations were calculated from $OD_{280}$ measurements using an extinction coefficient of 14280 $M^{-1}$ $cm^{-1}$.

**Preparation of Lipid Vesicles.** Lipids in chloroform were mixed in the appropriate molar ratio, dried under $N_2$, and then placed under vacuum for 2 h to remove all traces of solvent. Dried lipids were then hydrated with assay buffer. Small unilamellar vesicles (SUV) were then generated through probe sonication, stored at 4 °C for no more than 7 days, and allowed to equilibrate overnight at 25 °C prior to EPR measurement. Vesicle stock solutions for EPR were prepared with a POPC:POPS molar ratio of 75:25 and a total lipid concentration of 80 mM; vesicle stocks for kinetic measurements consisted of a 75:20:5 POPC:POPS:dansyl-PE molar ratio to maintain 25% anionic content, and a total lipid concentration of 3 mM.

**Stopped Flow Kinetic Measurements.** Membrane association and dissociation rates were measured using a BioLogic SFM-3000 stopped flow fluorescence spectrometer essentially as outlined previously.[37] Briefly, protein-to-membrane fluorescence resonance energy transfer (FRET) was measured between Trp residues in the C2 domain and dansyl-PE lipids included in vesicles. Association measurements were performed by rapidly mixing protein and vesicles in the presence of 200 μM $CaCl_2$, and dissociation measurements were performed following rapid addition of 1 mM EDTA to preformed protein−lipid complexes. Protein:accessible lipid ratios were maintained at 1:100 for kinetic measurements, including 1 μM protein and 100 μM total accessible lipid in all association measurements (all concentrations after mixing). Observed association rates were fit to equations of the form

$$F = \Delta F_{max}(1 - e^{-k_{obs}t}) + C \quad (1)$$

where $k_{obs}$ is the apparent association rate constant, $\Delta F_{max}$ is the amplitude of the fluorescence change, and $C$ is an offset. Dissociation profiles were subjected to nonlinear least-squares fitting to a single- or double-exponential function (eq 2 or 3, respectively):

$$F = \Delta F_{max}(1 - e^{-k_{off}t}) + C \quad (2)$$

$$F = \Delta F_{max1}(1 - e^{-k_{off1}t}) + \Delta F_{max2}(1 - e^{-k_{off2}t}) + C \quad (3)$$

where the $k_{off}$ terms are dissociation rate constants and $C$ is an offset. Except where otherwise noted, dissociation profiles for mutants were single-exponential.

**Measuring EPR Spectra.** An EPR spectrum was recorded for each single-cysteine variant using a Bruker ELEXSYS E500 spectrometer (9.4 GHz) with a loop gap resonator (Medical Advances). Each sample consisted of 30−150 μM MTSSL-labeled Syt7 C2A, 1.5−2.0 mM $CaCl_2$, and either no lipids present for unbound spectra or a 3:1 POPC/POPS lipid mixtures for bound spectra. Although this results in $Ca^{2+}$ concentrations higher than physiological (typically ∼10−500 μM, depending on cell type and stimulus), the C2A domain binds up to three $Ca^{2+}$ ions, so an at least 3-fold molar excess is required to saturate membrane binding.[40] A high total lipid concentration of 30 mM (15 mM accessible), similar to those of previous EPR studies,[25,41,42] was used to minimize the possibility of spin−spin interactions between the MTSSL tags of bound Syt7 C2A domains. This corresponds to a protein:accessible lipid ratio between 1:100 and 1:500. Measurements were performed at an incident power of 2.0 mW with a minimum of five scans of 100 G. EPR spectra were normalized to their second integral representing the total number of spins. This technique has proven to be effective in previous studies for comparing spectra of varying spin-label concentrations particularly when comparing bound and unbound states.[41,42]

**Continuous Wave Power Saturation Measurements.** Each sample was loaded into a gas-permeable TPX capillary tube (Medical Advances). Power saturation curves were measured between 0.2 and 50 mW taking saturation measurements at predefined intervals, over 30 G with at least two scans per interval. Power saturation curves for each sample were measured under three separate conditions: (1) atmospheric oxygen (20%), (2) after equilibration under $N_2$ for 15 min, and (3) after addition of 10 mM NiEDDA and equilibration under $N_2$ for 15 min. All three accessibility measurements for a single protein were taken on the same day to minimize slight variations in sample preparation and/or instrument (resonator) performance. The measurements include *n*-doxyl PC standards measured under the same conditions (temperature, buffer, and $[Ni^{2+}]$) that were used for the protein samples. Amplitudes were plotted as a function of microwave power squared and fit using Kaleidagraph to the equation[21,22]



DOI: 10.1021/acs.biochem.5b00421
*Biochemistry* 2015, 54, 5684−5695

$$A = CP^{0.5}\left[1 + \frac{(2^{1/\epsilon} - 1)P}{P_{1/2}}\right]^{-\epsilon} \quad (4)$$

where $A$ represents the peak-to-peak amplitude of the signal, $C$ is a scaling factor, $P$ is the microwave power, $P_{1/2}$ is the power at which half-saturation occurs, and $\epsilon$ is the measure of homogeneity of saturation. Accessibility parameters were then calculated as follows:[21,22]

$$\prod(\mathrm{X}) = \left[\frac{P_{1/2}(\mathrm{X})}{\Delta H_{pp}(\mathrm{X})}\right] - \left[\frac{P_{1/2}(\mathrm{N_2})}{\Delta H_{pp}(\mathrm{N_2})}\right] \quad (5)$$

where X represents either the $O_2$ or the NiEDDA paramagnetic species, $\Pi(X)$ represents the accessibility parameter for the given species, and $\Delta H_{pp}$ is the average peak to peak line width over the linear region of the power saturation curve. Depth parameters were then calculated from the following equation:

$$\Phi = \ln\left[\frac{\prod(\mathrm{O_2})}{\prod(\mathrm{NiEDDA})}\right] \quad (6)$$

where $\Phi$ is the depth parameter. Errors on each $\Pi$ and $\Phi$ measurement were calculated from the standard errors of $P_{1/2}$ and $\Delta H_{pp}$ values. The depth parameter was measured at least twice for each mutant and three times if the first two measurements differed by more than 0.4. Final values reported are weighted averages and the 95% confidence interval (CI) among repeat measurements.

**Modeling Docking Geometry.** The experimental membrane docking geometry for Syt7 C2A was determined by first modeling the locations of MTSSL spin labels and subsequently fitting to obtain a best-fit docking geometry based on the measured depth parameters for each spin-labeled mutant. Allowed configurations of MTSSL side chains were modeled using the MTSSL Wizard plugin for PyMol (Schrödinger).[43] Initial estimated coordinates for each nitroxide nitrogen (on which the free electron resides)[44] were determined by averaging the coordinates among all allowed conformations of the MTSSL tag. For the two to five positions at which no conformers were found using the "tight" settings of MTSSL Wizard, individual side-chain dihedral angles were defined manually to yield conformations with no structural clashes. These coordinates were then used for fitting depth parameters to a hyperbolic tangent function:

$$\Phi = A\tanh[B(d_m - C)] + D \quad (7)$$

where $A$ and $D$ represent the bulk values of $\Phi$ in water and hydrocarbon, respectively, $C$ sets the inflection point of the curve, $B$ determines the slope, and $d_m$ represents the distance of each MTSSL spin label from the phosphate plane. As in previous studies, fits were constrained such that $D - A = 4.5$. For doxyl lipid standards, $d_m$ is the published value,[45] and for MTSSL labels, $d_m$ is given by

$$d_m = x\sin(\theta_z) + y\cos(\theta_x) - z\cos(\theta_z)\sin(\theta_x) + y_{trans} \quad (8)$$

where $(x,y,z)$ are the starting coordinates of the MTSSL nitrogen for each side chain. Fitting of depth parameter data to eqs 7 and 8 yields an optimized docking geometry of the protein to a lipid bilayer in the $xz$ plane, where $y = 0$ is the average phosphate position of the proximal leaflet. This optimized docking geometry can be obtained by sequentially (1) rotating the coordinates around the $x$ axis by the best-fit angle $\theta_x$, (2) rotating the coordinates around the $z$ axis by the best-fit angle $\theta_z$, and (3) translating along the $y$ axis by the best-fit distance $y_{trans}$. After a first round of fitting using the average MTSSL coordinates, any residues that were outliers to the hyperbolic tangent fit (more than 2 × 95% CI from the predicted $\Phi$ value) were then sequentially adjusted to a defined side-chain conformation with dihedral angles ($\chi$) that were both (1) sterically allowed for the position and (2) low-energy based on a previous study of MTSSL conformations in solution.[46] Such adjustment was performed beginning with the farthest outliers and repeated until any further changes provided a negligible improvement to the fit. The following positions were those at which rotamer conformations were adjusted during the iterative fitting process: for structure A, G169, N195, and L196; for structure B, F167 and G169; for structure C, F167 and G169; for NMR state 1, F167, G169, and L196; and for NMR state 2, G169 and S168. The dihedral angles used for each final model are listed in Table S1; for the remaining majority of positions, the average coordinates from MTSSL Wizard were used. Five models were created using this method: three based on starting protein structures taken from a molecular dynamics simulation of $Ca^{2+}$-bound Syt7 C2A in the absence of a membrane [snapshots at 6, 8, and 10 ns of a simulation described in the following paper in this issue (DOI: 10.1021/acs.biochem.5b00422)] and two based on starting $Ca^{2+}$-free structures from the Protein Data Bank (entry 2D8K, states 1 and 2). Each final self-consistent model is constrained by eqs 7 and 8, experimental depth parameters, doxyl lipid calibration data, and the corresponding structure of Syt7 C2A.

Reanalysis of published Syt1 C2A EPR data was conducted analogously, starting with states 1−3 of structure 1BYN[47] as well as three snapshots of a molecular dynamics simulation described in the following paper in this issue (DOI: 10.1021/acs.biochem.5b00422); any manually adjusted dihedral angles are listed in Table S2.

## RESULTS

**Site Selection, Protein Purification, and MTSSL Labeling.** The process of protein site-directed spin labeling introduces an unpaired electron through the MTSSL nitroxide spin label (Figure 1). The spin label attaches through a disulfide bond to any accessible cysteine; therefore, native cysteine residues must first be removed to selectively label cysteine residues at the desired locations of interest. The only native cysteine in our wild-type expression construct was Cys260 near the C-terminus; this residue occurs at the beginning of the flexible C2A−C2B linker region in native human Syt7. A cysless (C260S) variant of Syt7 C2A was therefore generated as a template for the creation of single-cysteine mutants. The positions selected for site-directed spin labeling in Syt7 C2A are analogous to positions used in a previous EPR power saturation study with Syt1 C2A.[25] This strategy allows for direct comparisons between Syt7 and Syt1. Spin-labeled positions are summarized in Table 1 covering 16 sites on or near $Ca^{2+}$ binding loops 1 and 3 of Syt7 C2A, with one negative control (Q148R1) opposite the binding site.

WT, cysless, and single-cysteine mutants were purified through glutathione affinity chromatography of a GST-linked protein followed by cleavage of the GST with thrombin. Nucleic acid contamination was removed to a level deemed acceptable for stopped flow kinetic measurements, and more than sufficient for equilibrium EPR measurements (see Experimental Procedures). MTSSL spin labels were attached


DOI: 10.1021/acs.biochem.5b00421
Biochemistry 2015, 54, 5684−5695

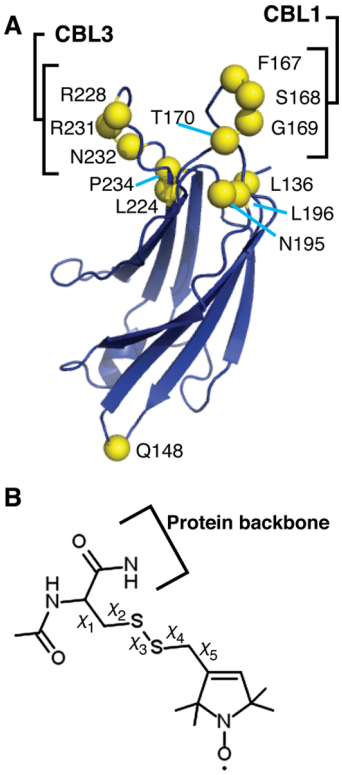


**Figure 1.** Spin labeling of Syt7 C2A. (A) Solution NMR structure of Syt7 C2A (PDB entry 2D8K). Yellow spheres indicate residues used for EPR spin-label measurements. (B) Structure of the MTSSL tag, with dihedral angles $\chi_1$–$\chi_5$ indicated.

either during or after purification, with a labeling efficiency of ≥75% in either case (Figure S1).

**Effects of Spin Labeling on Syt7 C2A Docking Function.** The methanethiosulfonate R1 spin label is a moderate-polarity group that has a minimal effect on the membrane protein docking structure as shown in previous EPR studies.[41,48] Here, we used an established protein-to-membrane FRET assay to examine the kinetics of membrane binding and dissociation of each spin-labeled mutant, for comparison to the wild-type and cysless Syt7 C2A. Spin-labeled mutants that produced association and dissociation rate constants within a factor of 2.7 relative to that of the C260S (cysless) mutant (equivalent to molar activation energies within the range ± *RT*) were considered to have negligible effects on docking and were used for EPR studies. Summarized in Table 1 are the off and on rates for the wild type, cysless, and each single-cysteine mutant.

The wild-type Syt7 C2A domain produced an observed association rate constant of 27 $s^{-1}$ and an EDTA-induced dissociation rate constant of 26 $s^{-1}$, using the liposomes here composed of 75% POPC, 20% POPS, and 5% dansyl-PE. This is a significantly slower association and somewhat faster dissociation than we reported previously for this protein domain and a more complex physiological lipid mixture.[37] These differences could arise from additional favorable interactions with other components of the physiological lipid mixture and are currently under investigation. However, we have also observed significant variability even with nominally identical lipid compositions, presumably because of batch differences in lipid stock concentration or homogeneity. The origins of this variability are currently under investigation. For the study presented here, all comparisons of on rates or off rates are between measurements made using the same preparation of liposomes. Cysless (C260S) exhibited dissociation ∼30% slower than and association ∼2-fold faster than those of the wild type. Viewed in the context of activation energies, 2-fold differences in rate constants are minor; moreover, C260 resides in a flexible C-terminal tail of the protein construct used for these experiments (and in the C2A–C2B linker of the full-length protein), so the difference in association rate is unlikely to represent a fundamental change in the C2A domain.

Nine of the mutants agreed within ≤2-fold of both the off and on rates for cysless. Four variants (G169R1, L196R1, L224R1, and Q148R1) had either on or off rates that were between 2- and 2.7-fold faster or slower than those of cysless. Two mutations, Y226R1 and A164R1, slowed association kinetics by >2.7-fold; the reason for the differences is unknown. F229R1 showed normal association kinetics but dissociated >2.7-fold faster than cysless, suggesting that this residue on the apex of CBL3 is essential for membrane penetration. One mutant (I235R1) had no observable kinetics, which could be due to the interior location of this residue causing the mutant protein to misfold; we note the purification yields of this mutant were also extremely low. Thus, these four mutations (F229R1, A164R1, Y226R1, and I235R1) were considered perturbing to the normal function of the Syt7 C2A protein and were excluded from further study. R228R1 and R231R1 were observed to have biphasic association profiles; however, in both of these cases, the faster component was within 2-fold of that of the wild type and had an amplitude >3-fold greater than that of the slow component. The origin of the slow, low-amplitude FRET increase upon binding is unclear but could arise from either (a) a small population that binds more slowly because of alternative folding or nucleic acid contamination, which would not impact EPR measurements significantly because of the high lipid concentrations and much longer measurement time scale (minutes to hours), or (b) slow vesicle aggregation, which would not affect EPR measurements because of the much smaller protein:lipid ratio used in EPR samples.

**EPR Line Shape Analysis.** As a qualitative measure of changes in the local environment around a spin label during membrane docking, continuous wave EPR spectra were measured for the 13 spin-labeled mutants included in the docking model. Both bound and unbound spectra were measured for each mutant and are shown in Figure 2. As a reference, doxyl lipid EPR spectra are displayed in Figure S2. Bound protein spectra included 3:1 POPC/POPS liposomes with a total lipid concentration of 30 mM and excess $Ca^{2+}$, conditions that allow for essentially complete membrane docking of Syt7 C2A. Unbound spectra were measured prior to addition of lipid but were otherwise equivalent to the corresponding bound sample.

The spin-labeled mutants of positions in CBL1 and CBL3 display the greatest degree of signal broadening in the bound state compared to the unbound state: F167R1, S168R1, G169R1, R228R1, and R231R1 (Figure 2). Signal broadening generally indicates decreased mobility of the MTSSL tag, likely in these cases because of contact with lipids as the CBLs penetrate the membrane. The remainder of the spin-labeled mutants showed varying degrees of signal broadening upon lipid addition, indicating lipid contact and/or loss of protein rotational freedom upon docking to the vesicles.

**Depth Parameters of Syt7 C2A.** EPR power saturation was performed to measure the depth parameters for each of the


DOI: 10.1021/acs.biochem.5b00421
*Biochemistry* 2015, 54, 5684–5695

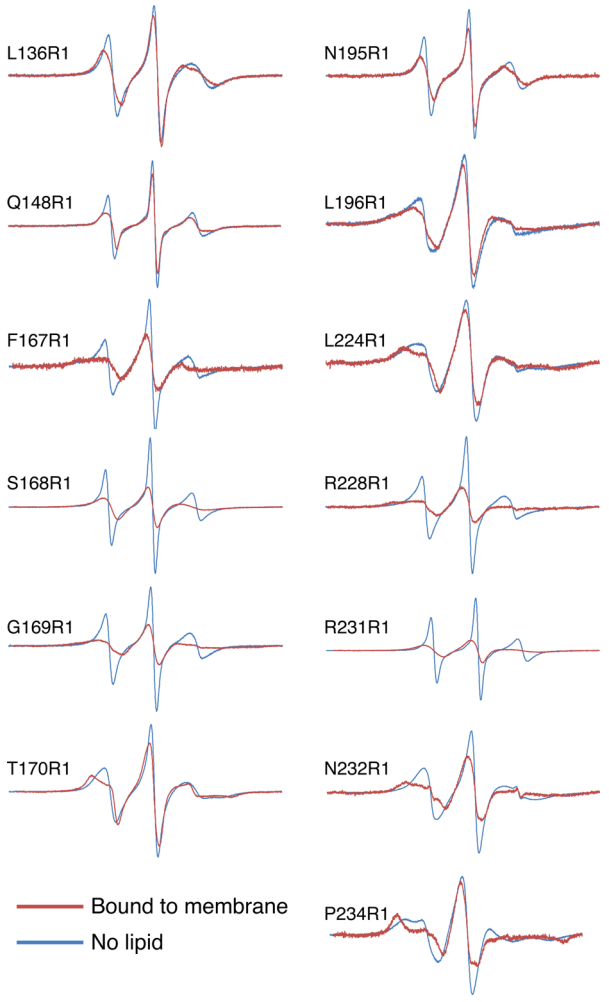


**Figure 2.** Bound and unbound EPR spectra for each spin-labeled mutant. Bound spectra (red) were measured with 30−150 $\mu$M protein and 30 mM (3:1 PC:PS) lipid membrane with 1.5−2.0 mM $Ca^{2+}$. Unbound spectra (blue) were measured with similar protein concentrations but in free solution with an identical $Ca^{2+}$ concentration. Signal broadening is indicative of a less mobile spin label.

13 spin-labeled positions on Syt7 C2A as well as four doxyl-PC lipids with spin-labeled acyl chains at carbons 5, 7, 10, and 12. Doxyl-PC lipids have a known depth within the lipid membrane and are useful in calibrating the hyperbolic tangent fit used to translate depth parameters into physical depths.[45] Table 2 summarizes the depth parameters along with the $O_2$ and NiEDDA accessibility parameters used to calculate the depth parameters. Positive depth parameters are indicative of more deeply penetrated spin labels, while depth parameters of less than −1 correspond to positions in the bulk aqueous phase.

Of the 13 Syt7 C2A mutants, seven showed depth parameters of less than −1 (L136R1, Q148R1, T170R1, N195R1, L196R1, L224R1, and P234R1), indicating aqueous exposed locations with little to no membrane contact. Three of the positions (F167R1, S168R1, and R228R1) had positive depth parameters, indicating membrane penetration potentially deeper than that in the phosphate plane of the lipid membrane. Three positions (G169R1, R231R1, and N232R1) had depth parameters between −1 and 0, suggesting proximity to the phosphate plane. Measured depth parameters for each doxyl lipid were in good agreement with previous literature values,

**Table 2. Probe Accessibility and Depth Parameters for Doxyl Lipids and Spin-Labeled C2A Domains**

| sample type | $\Pi(O_2)^a$ | $\Pi$(NiEDDA)$^a$ | $\Phi^b$ |
|---|---|---|---|
| L136R1 | 1.37 ± 0.10 | 7.39 ± 0.23 | −1.59 ± 0.18 |
| Q148R1 | 2.99 ± 0.24 | 12.66 ± 0.58 | −1.38 ± 0.21 |
| F167R1 | 3.19 ± 0.34 | 2.25 ± 0.31 | 0.27 ± 0.19 |
| S168R1 | 3.32 ± 0.21 | 1.06 ± 0.25 | 1.12 ± 0.30 |
| G169R1 | 2.18 ± 0.16 | 3.49 ± 0.26 | −0.43 ± 0.17 |
| T170R1 | 1.67 ± 0.49 | 12.01 ± 0.91 | −1.85 ± 0.40 |
| N195R1 | 1.86 ± 0.17 | 11.70 ± 0.59 | −1.83 ± 0.20 |
| L196R1 | 2.19 ± 0.31 | 14.55 ± 0.64 | −1.89 ± 0.21 |
| L224R1 | 1.41 ± 0.23 | 7.62 ± 0.42 | −1.54 ± 0.24 |
| R228R1 | 2.42 ± 0.25 | 0.92 ± 0.14 | 0.69 ± 0.24 |
| R231R1 | 1.55 ± 0.33 | 2.50 ± 0.24 | −0.48 ± 0.29 |
| N232R1 | 1.24 ± 0.24 | 3.57 ± 0.35 | −0.94 ± 0.46 |
| P234R1 | 0.96 ± 0.14 | 4.18 ± 0.23 | −1.42 ± 0.23 |
| Doxyl 5 | 4.48 ± 0.17 | 0.74 ± 0.09 | 1.73 ± 0.21 |
| Doxyl 7 | 5.97 ± 0.52 | 0.55 ± 0.15 | 2.42 ± 0.42 |
| Doxyl 10 | 7.53 ± 0.36 | 0.70 ± 0.12 | 2.42 ± 0.24 |
| Doxyl 12 | 9.03 ± 0.62 | 0.38 ± 0.16 | 3.13 ± 0.54 |

[a]Uncertainties reported as weighted averages from 95% confidence intervals derived from fits to power saturation curves as described in Experimental Procedures (eq 4). [b]Depth parameter uncertainties propagated from the accessibility parameters.

although these values can vary somewhat among spectrometers.[45]

Several of the Syt7 C2A depth parameters are considerably deeper than those reported previously for analogous positions in Syt1. For example, F167, G169, R228, and N232 are all positions on CBL1 or CBL3 that have depth parameters in Syt7 C2A of >1.0 more positive than the corresponding positions in Syt1 C2A (Table 3).[25] By comparison, depth parameters at non-CBL positions were greater in Syt7 C2A by a smaller magnitude of 0.4 ± 0.2, and doxyl-PC depth parameters were greater in our study by only 0.2 ± 0.2. Together, these data suggest that the CBLs of Syt7 C2A penetrate into membranes more deeply than those of Syt1 C2A, although determination of the docking geometry requires fitting these measured depth parameters onto a structural model.

**Modeled Docking Geometry of Syt7 C2A.** To translate depth parameters into physical distances from the membrane phosphate plane, a hyperbolic tangent model is used to determine a best-fit geometry based on the relationship between depth parameters and structure (Figure 3). The measured depth parameters were used to create a suite of structural models of the Syt7 C2A membrane docking geometry. Earlier EPR docking geometry studies of C2 domains have modeled geometries based on single static protein structures, and single conformations of the MTSSL side chain at each position. Both of these assumptions likely underrepresent the dynamics of membrane binding and produce relatively crude estimates of uncertainty in the final geometric model. In the case of Syt7 C2A, the available structure is an NMR ensemble of states from measurements performed in the absence of $Ca^{2+}$. Many of these states possess CBL structures that are not relevant to the $Ca^{2+}$-bound protein structure. Thus, we first performed molecular dynamics simulations of Syt7 C2A bound to three $Ca^{2+}$ ions (in the absence of a membrane), details of which are presented in the following paper in this issue (DOI: 10.1021/acs.biochem.5b00422). Three representative snapshots from this


DOI: 10.1021/acs.biochem.5b00421
Biochemistry 2015, 54, 5684−5695

**Table 3. Average Spin-Label Depths from Three Docking Models of $Ca^{2+}$-Bound Syt7 C2A, Compared to Previously Published Values for Syt1 C2A**

| mutant | Φ[a] | average spin-label depth (Å)[b] | equivalent residue in Syt1[c] | Syt1 C2A Φ[d] |
|---|---|---|---|---|
| L136R1 | −1.59 ± 0.18 | −12.5 ± 9.3 | L142 | −1.9 |
| Q148R1 | −1.38 ± 0.21 | −36.2 ± 2.8 | Q154 | ND |
| F167R1 | 0.27 ± 0.19 | 4.0 ± 0.2 | M173 | −1.4 |
| S168R1 | 1.12 ± 0.30 | 6.2 ± 0.7 | G174 | 0.4 |
| G169R1 | −0.43 ± 0.17 | 0.8 ± 1.3 | G175 | −1.8 |
| T170R1 | −1.85 ± 0.40 | −6.4 ± 2.6 | T176 | −1.9 |
| N195R1 | −1.83 ± 0.20 | −8.2 ± 0.7 | T201 | −1.9 |
| L196R1 | −1.89 ± 0.21 | −8.8 ± 3.1 | L202 | −2.4 |
| L224R1 | −1.54 ± 0.24 | −5.4 ± 2.8 | Y229 | −2.0 |
| R228R1 | 0.69 ± 0.24 | 5.2 ± 0.5 | R233 | −1.4 |
| R231R1 | −0.48 ± 0.29 | 1.3 ± 1.0 | K236 | −0.6 |
| N232R1 | −0.94 ± 0.46 | −2.7 ± 1.7 | H237 | −2.0 |
| P234R1 | −1.42 ± 0.23 | −7.3 ± 2.3 | I239 | −2.1 |
| Doxyl 5 | 1.73 ± 0.21 | 8.1[e] | | 1.45[e] |
| Doxyl 7 | 2.42 ± 0.42 | 10.5[e] | | 2.05[e] |
| Doxyl 10 | 2.42 ± 0.24 | 14.0[e] | | 2.42[e] |
| Doxyl 12 | 3.13 ± 0.54 | 16.0[e] | | 2.82[e] |

[a]From Table 2. [b]Mean ± SD of the spin-label nitrogen depth from three structural models based on simulations of Syt7 C2A bound to three $Ca^{2+}$ ions, created as described in the text. Depths from individual structural models are listed in Table S3. [c]Determined from alignment of amino acid sequences for Syt1−Syt10 using Clustal Omega. [d]From ref 25. [e]Previously published values for doxyl lipids.[45]

simulation, which we term structures A−C, were used as bases for fitting depth parameter data, and the depths reported in Tables 3 and 4 are averages among these three fits. For comparison, states 1 and 2 from the available $Ca^{2+}$-free NMR structure (termed NMR1 and NMR2, respectively) were also used as bases for fitting; depths from all five fits are listed in Table S3. The results provide five self-consistent docking geometries, each modeled using the same set of depth parameter data but with a different starting protein structure.

In each case, modeling consisted of three steps as in previous studies: (1) estimation of coordinates for the MTSSL tag at each position relative to the starting protein structure, (2) fitting of depth parameter data to a hyperbolic tangent function to obtain docking geometry parameters, and (3) iterative adjustment of the MTSSL side-chain conformation at selected positions to improve self-consistent fitting.

While previous studies have estimated initial MTSSL coordinates by assigning a single rotamer conformation at each position, we instead assigned initial coordinates based on the average coordinates among allowed rotamers at each position, using the recently developed MTSSL Wizard plugin for Pymol.[43] Exceptions were (a) positions at which the "tight" setting of the MTSSL Wizard yielded no predicted rotamers and (b) positions that were defined as particular rotamers during the iterative fitting process to improve fitting to the hyperbolic tangent function. In either case, rotamers that matched previously described energy minima for the MTSSL side chain and produced no obvious steric clashes were chosen.[46] For example, T170 is located in a shallow groove that produced no rotamers in structures 1 and 3 using MTSSL Wizard; however, it was accommodated by $\chi_1$ and $\chi_2$ angles of −60° ($g^+$, $g^+$). The positions whose rotamer conformations were adjusted during the iterative fitting process are listed in Experimental Procedures, and the dihedral angles used for these positions are listed in Table S1.

As in previous EPR depth studies of Syt1 C2 domains, depth parameter data were fit to a hyperbolic tangent function empirically shown to model depth parameter measurements as a function of insertion depth.[25,26] Depth parameter varies approximately linearly with penetration depth in the membrane interior but is independent of the distance from the membrane surface for positions that are highly aqueous. Doxyl lipid standards with a known penetration depth were used to calibrate the slope of the curve in the membrane interior (empty circles in Figure 3). The self-consistent best-fit relationship between depth parameter and distance fit to eqs 7 and 8 is shown in Figure 3A−E for all five starting structural models. The fit includes three parameters defining the curve shape ($A$, $B$, and $C$ in eq 7) and three parameters defining the penetration and orientation of the C2A domain with respect to the membrane ($y_{trans}$, $\theta_x$, and $\theta_z$ in eq 8). The protein−membrane docking geometry is then achieved by sequentially rotating the starting protein coordinates by Euler angles $\theta_x$ and $\theta_z$ and then translating by $y_{trans}$. These transformations produce a docked protein structure in which the $x$−$z$ plane represents the average phosphate position of a planar membrane. The five orientations obtained from this method are shown in Figure 4.

The use of five starting structures (three containing $Ca^{2+}$ and two without) offers a glimpse into the uncertainty associated with modeling the docking geometry by this method. Loops and external side chains on a protein have considerably more flexibility than a single static crystal structure. $Ca^{2+}$-bound structure A and NMR state 2 produced the shallowest penetration depths, while $Ca^{2+}$-bound structure C and NMR state 1 produced the deepest. The distance of each spin label from the membrane phosphate plane in each model is listed in Table S3, and the averages among the three $Ca^{2+}$-bound geometries are listed in Table 3. As expected from the hyperbolic curve fit, the more aqueous positions had a larger uncertainty associated with their position. The standard deviations were generally in the range of 0−3 Å, comparable to previously estimated uncertainties associated with EPR depth parameter measurements,[25,42] with the exception of L136, which resides on the flexible and solvent-exposed N-terminus of the domain.

For a consistent comparison of the Syt7 and Syt1 C2A docking geometries, we also reanalyzed the published Syt1 C2A depth parameters[25] using the same methods that were used in our Syt7 C2A analysis. A suite of Syt1 C2A docking geometry models were created, including (a) mapping MTSSL side-chain configurations using average positions from MTSSL Wizard and (b) using six Syt1 C2A structures as bases for fitting: states 1−3 from the published NMR structure of the $Ca^{2+}$-loaded domain[47] and three snapshots from a molecular dynamics simulation of the $Ca^{2+}$-loaded domain [described in the following paper in this issue (DOI: 10.1021/acs.biochem.5b00422)]. All six of these models are shallower than the previously reported Syt1 C2A docking geometry (Table 4, Figures S3 and S4, and Table S4). The discrepancy can be attributed mainly to differences in the MTSSL side-chain geometries used for fitting, particularly for two positions in CBL3, as discussed further in the legend of Figure S4. Thus, comparing docking geometries using the same modeling approach further indicates that Syt7 C2A inserts deeper than Syt1 C2A.



DOI: 10.1021/acs.biochem.5b00421
*Biochemistry* 2015, 54, 5684−5695

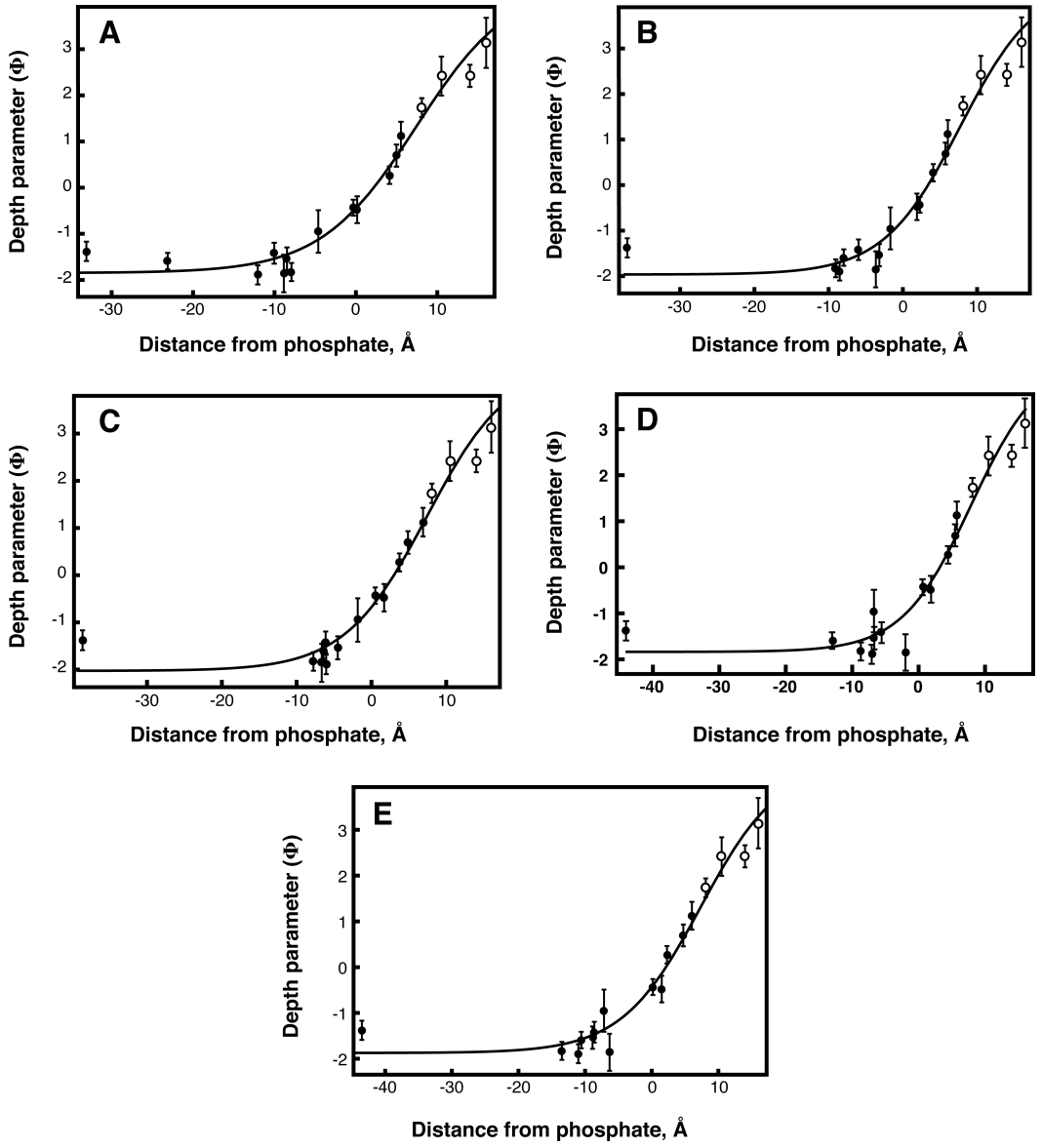


**Figure 3.** Hyperbolic tangent fits of experimentally determined Syt7 C2A depth parameters. Empty circles indicate data for doxyl lipids, and filled circles indicate data for single-cysteine mutants. Each fit is based on eqs 7 and 8. Error bars are the 95% CI of depth parameter values measured in duplicate or triplicate, which are listed in Table 2. The same depth parameter data were used for each fit, and applied to (A) $Ca^{2+}$-bound structure A, (B) $Ca^{2+}$-bound structure B, (C) $Ca^{2+}$-bound structure C, (D) NMR structure state 1, or (E) NMR structure state 2. The relevant NMR structure is PDB entry 2D8K.

**Table 4. Comparison of α-Carbon Depths between Syt7 C2A and Syt1 C2A**

| residue | Syt7 C2A (Å)[a] | equivalent residue in Syt1[b] | Syt1 C2A, reported (Å)[a,c] | Syt1 C2AB, reported (Å)[a,d] | Syt1 C2A, reanalysis (Å)[a,e] | Syt1 C2A, reanalysis (Å)[a,f] |
|---|---|---|---|---|---|---|
| D166 | 0.0 ± 1.8 | D172 | −1.4 | 4.5 | −2.9 ± 1.0 | −4.4 ± 0.3 |
| F167 | 2.4 ± 2.1 | M173 | 0.8 | 7.0 | −0.3 ± 1.3 | −1.7 ± 0.2 |
| S168 | 1.9 ± 1.7 | G174 | −0.7 | 4.6 | −1.9 ± 0.7 | −2.6 ± 0.4 |
| G169 | −1.6 ± 1.9 | G175 | −4.5 | 1.8 | −5.3 ± 0.8 | −6.3 ± 0.4 |
| D227 | 0.3 ± 0.8 | D232 | 0.3 | 2.8 | −4.1 ± 0.9 | −4.5 ± 0.1 |
| R228 | 2.5 ± 0.4 | R233 | 2.6 | 2.9 | −2.9 ± 0.4 | −3.0 ± 0.4 |
| F229 | 5.5 ± 0.8 | F234 | 5.3 | 6.3 | 0.6 ± 0.4 | 0.5 ± 0.2 |
| S230 | 3.8 ± 1.3 | S235 | 4.0 | 7.3 | 0.4 ± 0.8 | −0.4 ± 0.5 |
| R231 | 0.4 ± 1.2 | K236 | 0.8 | 5.4 | −2.0 ± 0.8 | −3.4 ± 0.6 |

[a]Distance from α-carbon to phosphate plane (positive values deeper). Data are means ± SD from models using three snapshots from molecular dynamics simulations of the $Ca^{2+}$-loaded domain as starting structures. [b]Determined from alignment of amino acid sequences for Syt1−Syt10 using Clustal Omega. [c]From ref 25. [d]From ref 27. [e]Mean ± SD using 1BYN states 1−3 as starting structures. [f]Mean ± SD using simulation snapshots as starting structures.



DOI: 10.1021/acs.biochem.5b00421
*Biochemistry* 2015, 54, 5684−5695

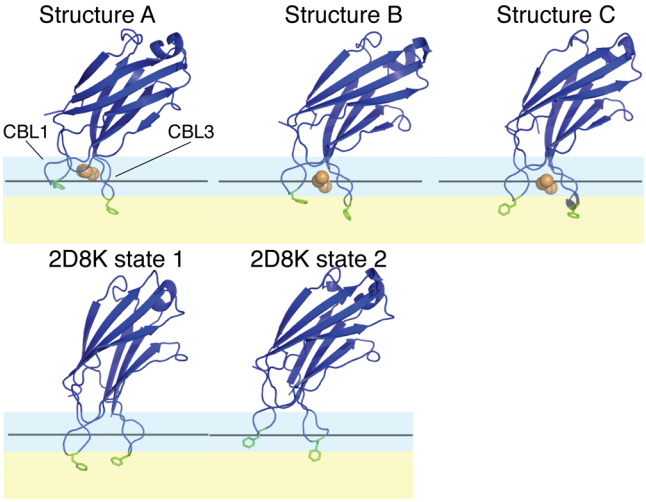


**Figure 4.** Optimized best-fit docking models for Syt7 C2A based on the indicated starting structure. Black lines represent the lipid phosphate plane; blue shading represents the approximate headgroup region, and yellow shading represents the approximate nonpolar acyl-chain region. The phenylalanine residues at positions 167 and 229 are colored green, and bound $Ca^{2+}$ ions are colored orange. Protein orientations correspond to successive Euler angle rotations of $\theta_x$ and $\theta_z$ followed by a translation along the $y$ axis of $y_{trans}$, as follows: structure A, $\theta_x = 252.8°$, $\theta_z = -4.4°$, $y_{trans} = -18.2$ Å; structure B, $\theta_x = 268.6°$, $\theta_z = 11.1°$, $y_{trans} = -16.8$ Å; structure C, $\theta_x = 261.8°$, $\theta_z = 14.7°$, $y_{trans} = -17.1$ Å; 2D8K state 1, $\theta_x = 17.5°$, $\theta_z = 4.8°$, $y_{trans} = -20.6$ Å; 2D8K state 2, $\theta_x = 23.1°$, $\theta_z = -6.4°$, $y_{trans} = -22.2$ Å. Starting coordinates for structures A–C are available in the Supporting Information.

Table 4 also compares our modeled Syt7 C2A penetration depths to previously published geometries for Syt1 C2A.[25] Notably, $\alpha$-carbons in CBL1 penetrate 1–5 Å deeper into the membrane for Syt7 C2A relative to all of the models for the isolated Syt1 C2A domain, consistent with the greater average depth parameter values of Syt7 C2A for positions in this loop. Regardless of which Syt1 C2A model is more accurate, these data are consistent with our earlier prediction that CBL1 of Syt7 C2A penetrates deeper than the corresponding region of Syt1 C2A.[37]

## DISCUSSION

EPR depth parameter measurements are useful for measuring docking geometries of peripheral membrane proteins, with uncertainties previously reported in the range of 2–3 Å.[25,42] Here, we note three significant findings from our EPR depth parameter study of Syt7 C2A. (i) The domain penetrates membranes somewhat more deeply than the isolated Syt1 C2A domain, although less deeply than Syt1 C2A in the C2AB tandem. (ii) Uncertainty in docking geometry models arises in large part because of inherent uncertainties in mapping side-chain depth parameters onto static protein structures. (iii) Hydrophobic effects appear to be more critical in CBL3 than in CBL1 for Syt7 C2A membrane docking, as the R1 spin label is less perturbing in place of Phe167 than at Phe229.

**Comparing Syt7 and Syt1 C2A Docking Models.** The extensive body of research detailing the structure and mechanism of Syt1 provides a valuable reference point for studies of other isoforms. The Syt7 C2A domain is known to bind membranes with a much greater $Ca^{2+}$ sensitivity and with dissociation kinetics significantly slower than those of its counterpart from Syt1.[37,49] Previously, we proposed a membrane docking mechanism for Syt7 C2A to explain this observation, in which an initial electrostatic association is followed by penetration of Phe residues in both CBL1 and CBL3 into the hydrophobic interior of the lipid membrane.[37] The depth measurements presented here are consistent with this hypothesis. Of the five Syt7 C2A docking geometry models shown in Figure 4, three show penetration of both Phe167 and Phe229 into the acyl-chain region of the membrane. The model for $Ca^{2+}$-bound structure B represents the median depth among the five and has depths closely similar to the mean of the three $Ca^{2+}$-bound structures (Table 3 and Table S3).

A comparison of previously published EPR docking geometries for Syt1 C2A to our suite of models for Syt7 C2A shows consistent and nearly equal penetration of CBL3 but variable penetration of CBL1.[25] Two previous depth parameter studies have been conducted for Syt1 C2A: one with the isolated domain and one in the C2AB tandem.[25,27] Figure 5 and

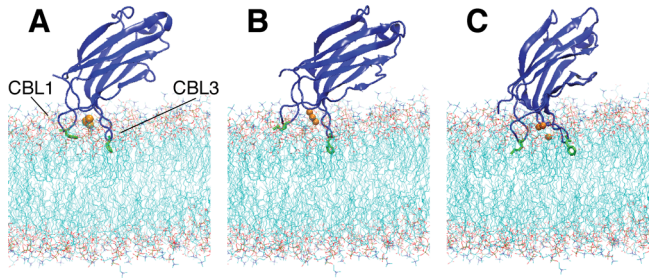


**Figure 5.** Comparison of (A) the median Syt7 C2A docking geometry determined here (structure B in Figure 4) with (B) the reported Syt1 C2A docking geometry of the isolated domain[25] and (C) the reported Syt1 C2A docking geometry in the C2AB tandem.[27] Optimized docking geometries are superimposed on a simulated lipid bilayer containing 25% POPS and 75% POPC. Hydrophobic side chains on CBL1 and CBL3 are colored green, and $Ca^{2+}$ ions are colored orange. Syt1 C2A geometries are reconstructed on the basis of the transformations reported previously.[25,27]

Figure S3 show side-by-side comparisons of our structure B docking geometry to these two previously reported docking geometries of Syt1 C2A, and Table 4 lists average $\alpha$-carbon depths for our $Ca^{2+}$-bound Syt7 C2A models compared to the four models of Syt1 C2A (two previously reported and two averages based on our reanalysis of the depth parameter data). The $\alpha$-carbon at the apex of CBL1 (Phe167 of Syt7 and Met173 of Syt1) increases in depth from 0.8 to 7.0 Å between isolated Syt1 C2A and Syt1 C2AB and ranges from 0.2 to 4.3 Å in our $Ca^{2+}$-bound Syt7 C2A models. By contrast, $\alpha$-carbon depths for the hydrophobic apex of CBL3 (Phe229 of Syt7 and Phe234 of Syt1) fall within a relatively narrow range of 4.6–6.0 Å in our $Ca^{2+}$-bound models, comparable to 5.3 Å in isolated Syt1 C2A and 6.3 Å in Syt1 C2AB. Direct comparison of depth parameters along with our reanalysis of the isolated Syt1 C2A data raises the possibility that CBL3 depth may also differ between the two domains (Tables 3 and 4 and Figure S4); thus, this comparison remains uncertain. Overall, our modeling shows a penetration depth of Syt7 C2A in which both CBL1 and CBL3 penetrate similarly or up to a few angstroms deeper in Syt7 C2A than in isolated Syt1 C2A.

**Uncertainty in Docking Geometry Modeling.** Because EPR-based models are useful in directly visualizing docking geometries of peripheral membrane proteins, it is important to understand the origins and extent of uncertainty in the


DOI: 10.1021/acs.biochem.5b00421
*Biochemistry* 2015, 54, 5684–5695

modeling process. Prior studies have reported estimated uncertainties in insertion depths, but the contributions from different stages of the measurement and modeling process have not formally been evaluated, to the best of our knowledge. Potential sources of uncertainty include (i) experimental measurements of depth parameters of spin-labeled protein mutants, (ii) prediction of spatial coordinates for each unpaired electron with respect to the protein backbone, and (iii) fits of the measured depth parameters and coordinates to a function that describes its docking geometry. Approaches for parts (ii) and (iii) have varied since the development of EPR depth measurements in the 1990s, including modern methods that combine fitting with molecular simulation, e.g., via simulated annealing.[31,50] The study presented here was designed to compare results with those of a 2003 study of Syt1 C2A, and therefore, we have used structure fitting and modeling protocols from that study where possible and adapted those methods when necessary. As a result, we have taken a somewhat novel approach for part (ii), which reveals a significant contribution to the uncertainty of the final model. Two novel components of our modeling approach are described below.

First, because the only available structure of Syt7 C2A lacks $Ca^{2+}$, we simulated the $Ca^{2+}$-bound protein domain in isolation for use as a reference structure. We used three snapshots from this simulation along with two different states of the available $Ca^{2+}$-free NMR structure as bases for modeling rather than a single protein structure as in most previous studies. This approach may capture effects of dynamic heterogeneity in the backbone structure of the CBLs that are responsible for membrane insertion. The range of docking geometries shown in Figure 4, each generated using the same depth parameter measurements and fitting method but using different side-chain and backbone structures, illustrates the contribution of starting protein structure to the final model. Modeled penetration depths for individual residues in CBL1 varied with standard deviations of ∼2 Å, while depths in CBL3 had smaller standard deviations of ∼1 Å (Table 4).

Second, we modeled coordinates of each unpaired electron relative to each protein structure largely by averaging coordinates among many possible side-chain rotamers, rather than from a single rotamer at each position as has been the standard practice in previous studies. The MTSSL Wizard tool was previously developed for double electron−electron resonance (DEER) distance measurements but to the best of our knowledge has not previously been used for membrane depth studies.[43] This approach streamlines the modeling process and reflects average side-chain configurations in a protein more accurately than a single rotamer, although it is limited by not scoring free energies of the available configurations. We reverted to the historical method of defining a single rotamer at positions for which sterics of other side chains limited the coordinate space available for the MTSSL side chain (for which MTSSL Wizard produced no rotamers using the "tight" definition of allowable contacts).

We also adopted a standard practice of defining and adjusting rotamer conformations for a few positions that did not fit well to the hyperbolic function using the average-position method.[21,41,42] In particular, we manually adjusted the side-chain configurations of F167R1 and/or G169R1 in each of the structural models, to account for the fact that these mutants have approximately equal depth parameters despite different positions in CBL1: Phe167 is at the apex of the loop, whereas Gly169 should be much less deeply inserted. We can account for the depth parameter data by defining the side-chain geometries such that the F167R1 side chain is oriented parallel to the membrane surface and/or G169R1 is oriented toward the membrane interior. While these orientations might be preferred by the protein, an alternative explanation is that the adjustments compensate for other sources of error such as minor effects of mutations on penetration depth. For example, the R1 side chain has a polarity intermediate between those of Gly and Phe; therefore, the F167R1 mutant has a more polar CBL1 and may penetrate less deeply, while G169R1 and S168R1 have more nonpolar CBL1 sequences and may penetrate more deeply. A similar effect may exist in Syt1 C2A with M173R1 and G174R1, both of whose side-chain positions had to be manually defined to $(\chi_1, \chi_2) = (g^+, g^+)$ in our reanalysis of these docking geometries. The fact that none of these mutations has a dramatic effect on membrane binding kinetics may reflect a secondary importance of CBL1 in membrane docking as discussed below.

**Roles of CBL1 and CBL3 in Membrane Docking of Syt7 C2A.** The differences in membrane binding and release kinetics between the F229R1 and F167R1 mutants may provide insight into the respective roles of CBL3 and CBL1 in Syt7 C2A. Phe229 in CBL3 appears to be essential to proper membrane binding, as its mutation to R1 leads to a 4-fold increased off rate relative to that of the cysless form of the domain (Table 1). In contrast, kinetics were not significantly impacted by mutation of Phe167 to cysteine and addition of an MTSSL spin label. The different effects of mutating these residues may indicate a more essential role for CBL3 compared to that of CBL1 in the membrane-docked structure.

On the basis of the relative tolerance of CBL1 to mutation and its greater uncertainty in penetration depth, it is tempting to speculate that this binding loop experiences greater structural dynamics in the membrane-bound state. However, the depth parameter is an ensemble average measurement and does not itself provide information about the dynamics of these loops. Lineshape analysis shows that individual side chains become more restricted upon membrane binding but is also not informative regarding overall tilting dynamics of the protein in the membrane. To resolve the uncertainty in penetration depth of CBL1 and to gain information about the relative energetics of CBL1 and CBL3 insertion, alternative approaches are necessary. In the following paper in this issue (DOI: 10.1021/acs.biochem.5b00422), we describe all-atom simulations of Syt7 C2A membrane docking that provide insight into these outstanding questions.

## ■ ASSOCIATED CONTENT

### Supporting Information

The Supporting Information is available free of charge on the ACS Publications website at DOI: 10.1021/acs.biochem.5b00421.

Side-chain dihedral angles used in Syt7 C2A modeling (Table S1), side-chain dihedral angles used in Syt1 C2A reanalysis (Table S2), final spin-label depths from the 5 Syt7 C2A docking models (Table S3), final spin-label depths from the six Syt1 C2A docking models (Table S4), efficiency of spin labeling (Figure S1), EPR spectra of doxyl lipids (Figure S2), hyperbolic fits from reanalysis of Syt1 C2A depth parameters (Figure S3), docking geometries from Syt1 C2A reanalysis (Figure S4), and



DOI: 10.1021/acs.biochem.5b00421
Biochemistry 2015, 54, 5684−5695

comparison of Syt1 and Syt7 docking geometries using cartoon representations of the membrane (Figure S5) (PDF)

PDB files of the six snapshots from simulations used as starting points for structural modeling:

PDB for Struture A (PDB)

PDB for Struture B (PDB)

PDB for Struture C (PDB)

PDB for Struture D (PDB)

PDB for Struture E (PDB)

PDB for Struture F (PDB)

## AUTHOR INFORMATION


### Corresponding Author

*Department of Chemistry, University of Colorado Denver, Campus Box 194, P.O. Box 173364, Denver, CO 80217. Phone: 303-556-6639. E-mail: jefferson.knight@ucdenver.edu.



### Funding

This work was supported by Multi-Investigator Cottrell College Science Award 22399 from the Research Corporation for Science Advancement to J.D.K. and H.L. and by National Institutes of Health (NIH) Grant R15GM102866 to J.D.K. Support for F.A.M. included an undergraduate fellowship through the Building Research Achievement in Neuroscience program [NIH Award R25GM097633 to Profs. Diego Restrepo (University of Colorado Denver, Aurora, CO) and Elba Serrano (New Mexico State University, Las Cruces, NM)].


### Notes

The authors declare no competing financial interest.

## ACKNOWLEDGMENTS


We thank Dr. Annette Erbse for expert assistance with EPR and for critical reading of the manuscript and Drs. Brian Ziemba and Joseph Falke for guidance on docking geometry modeling.


## ABBREVIATIONS

Syt, synaptotagmin; EPR, electron paramagnetic resonance; $PIP_2$, phosphatidylinositol 4,5-bisphosphate; WT, wild type; NiEDDA, nickel ethylenediaminediacetic acid; EDTA, ethylenediaminetetraacetic acid; POPC, 1-palmitoyl-2-oleoyl-*sn*-glycero-3-phosphocholine; POPS, 1-palmitoyl-2-oleoyl-*sn*-glycero-3-phospho-L-serine; SNARE, soluble *N*-ethylmaleimide-sensitive fusion protein attachment receptor; FRET, fluorescence resonance energy transfer; PH, pleckstrin homology; GRP1, general receptor of phosphoinositides 1; PKC$\alpha$, protein kinase C$\alpha$; DMF, dimethylformamide; $cPLA_2$, cytosolic phospholipase $A_2$; IPTG, isopropyl $\beta$-D-thiogalactopyranoside; SDS−PAGE, sodium dodecyl sulfate−polyacrylamide gel electrophoresis; HEPES, (4-(2-hydroxyethyl)-1-piperazineethanesulfonic acid; SUV, small (sonicated) unilamellar vesicle(s); PDB, Protein Data Bank; MTSSL, methanethiosulfonate spin label.

## REFERENCES


(1) Chapman, E. R. (2008) How does synaptotagmin trigger neurotransmitter release? *Annu. Rev. Biochem. 77*, 615−641.

(2) Martens, S., and McMahon, H. T. (2008) Mechanisms of membrane fusion: disparate players and common principles. *Nat. Rev. Mol. Cell Biol. 9*, 543−556.

(3) Corbalan-Garcia, S., and Gomez-Fernandez, J. C. (2014) Signaling through C2 domains: more than one lipid target. *Biochim. Biophys. Acta, Biomembr. 1838*, 1536−1547.

(4) Gustavsson, N., and Han, W. (2009) Calcium-sensing beyond neurotransmitters: functions of synaptotagmins in neuroendocrine and endocrine secretion. *Biosci. Rep. 29*, 245−259.

(5) Sugita, S., Shin, O. H., Han, W., Lao, Y., and Sudhof, T. C. (2002) Synaptotagmins form a hierarchy of exocytotic $Ca^{2+}$ sensors with distinct $Ca^{2+}$ affinities. *EMBO J. 21*, 270−280.

(6) Bhalla, A., Chicka, M. C., and Chapman, E. R. (2008) Analysis of the synaptotagmin family during reconstituted membrane fusion. Uncovering a class of inhibitory isoforms. *J. Biol. Chem. 283*, 21799−21807.

(7) Rickman, C., Craxton, M., Osborne, S., and Davletov, B. (2004) Comparative analysis of tandem C2 domains from the mammalian synaptotagmin family. *Biochem. J. 378*, 681−686.

(8) Hurley, J. H., and Misra, S. (2000) Signaling and subcellular targeting by membrane-binding domains. *Annu. Rev. Biophys. Biomol. Struct. 29*, 49−79.

(9) Schiavo, G., Gu, Q. M., Prestwich, G. D., Sollner, T. H., and Rothman, J. E. (1996) Calcium-dependent switching of the specificity of phosphoinositide binding to synaptotagmin. *Proc. Natl. Acad. Sci. U. S. A. 93*, 13327−13332.

(10) Bai, J., Tucker, W. C., and Chapman, E. R. (2004) $PIP_2$ increases the speed of response of synaptotagmin and steers its membrane-penetration activity toward the plasma membrane. *Nat. Struct. Mol. Biol. 11*, 36−44.

(11) Damer, C. K., and Creutz, C. E. (1994) Synergistic membrane interactions of the two C2 domains of synaptotagmin. *J. Biol. Chem. 269*, 31115−31123.

(12) Arac, D., Chen, X., Khant, H. A., Ubach, J., Ludtke, S. J., Kikkawa, M., Johnson, A. E., Chiu, W., Sudhof, T. C., and Rizo, J. (2006) Close membrane-membrane proximity induced by $Ca^{2+}$-dependent multivalent binding of synaptotagmin-1 to phospholipids. *Nat. Struct. Mol. Biol. 13*, 209−217.

(13) Choi, U. B., Strop, P., Vrljic, M., Chu, S., Brunger, A. T., and Weninger, K. R. (2010) Single-molecule FRET-derived model of the synaptotagmin 1-SNARE fusion complex. *Nat. Struct. Mol. Biol. 17*, 318−324.

(14) Krishnakumar, S. S., Kummel, D., Jones, S. J., Radoff, D. T., Reinisch, K. M., and Rothman, J. E. (2013) Conformational dynamics of calcium-triggered activation of fusion by synaptotagmin. *Biophys. J. 105*, 2507−2516.

(15) Martens, S. (2010) Role of C2 domain proteins during synaptic vesicle exocytosis. *Biochem. Soc. Trans. 38*, 213−216.

(16) Segovia, M., Ales, E., Montes, M. A., Bonifas, I., Jemal, I., Lindau, M., Maximov, A., Sudhof, T. C., and Alvarez de Toledo, G. (2010) Push-and-pull regulation of the fusion pore by synaptotagmin-7. *Proc. Natl. Acad. Sci. U. S. A. 107*, 19032−19037.

(17) Paddock, B. E., Wang, Z., Biela, L. M., Chen, K., Getzy, M. D., Striegel, A., Richmond, J. E., Chapman, E. R., Featherstone, D. E., and Reist, N. E. (2011) Membrane penetration by synaptotagmin is required for coupling calcium binding to vesicle fusion in vivo. *J. Neurosci. 31*, 2248−2257.

(18) Striegel, A. R., Biela, L. M., Evans, C. S., Wang, Z., Delehoy, J. B., Sutton, R. B., Chapman, E. R., and Reist, N. E. (2012) Calcium binding by synaptotagmin's C2A domain is an essential element of the electrostatic switch that triggers synchronous synaptic transmission. *J. Neurosci. 32*, 1253−1260.

(19) Hui, E., Johnson, C. P., Yao, J., Dunning, F. M., and Chapman, E. R. (2009) Synaptotagmin-mediated bending of the target membrane is a critical step in $Ca^{2+}$-regulated fusion. *Cell 138*, 709−721.

(20) Altenbach, C., Flitsch, S. L., Khorana, H. G., and Hubbell, W. L. (1989) Structural studies on transmembrane proteins. 2. Spin labeling of bacteriorhodopsin mutants at unique cysteines. *Biochemistry 28*, 7806−7812.

(21) Malmberg, N. J., and Falke, J. J. (2005) Use of EPR power saturation to analyze the membrane-docking geometries of peripheral proteins: applications to C2 domains. *Annu. Rev. Biophys. Biomol. Struct. 34*, 71−90.




DOI: 10.1021/acs.biochem.5b00421
*Biochemistry* 2015, 54, 5684−5695

(22) Altenbach, C., Greenhalgh, D. A., Khorana, H. G., and Hubbell, W. L. (1994) A collision gradient method to determine the immersion depth of nitroxides in lipid bilayers: application to spin-labeled mutants of bacteriorhodopsin. *Proc. Natl. Acad. Sci. U. S. A. 91*, 1667−1671.
(23) Almers, W. (1994) Synapses. How fast can you get? *Nature 367*, 682−683.
(24) Sudhof, T. C. (2013) Neurotransmitter release: the last millisecond in the life of a synaptic vesicle. *Neuron 80*, 675−690.
(25) Frazier, A. A., Roller, C. R., Havelka, J. J., Hinderliter, A., and Cafiso, D. S. (2003) Membrane-bound orientation and position of the synaptotagmin I C2A domain by site-directed spin labeling. *Biochemistry 42*, 96−105.
(26) Rufener, E., Frazier, A. A., Wieser, C. M., Hinderliter, A., and Cafiso, D. S. (2005) Membrane-bound orientation and position of the synaptotagmin C2B domain determined by site-directed spin labeling. *Biochemistry 44*, 18−28.
(27) Herrick, D. Z., Sterbling, S., Rasch, K. A., Hinderliter, A., and Cafiso, D. S. (2006) Position of synaptotagmin I at the membrane interface: cooperative interactions of tandem C2 domains. *Biochemistry 45*, 9668−9674.
(28) Bai, J., Wang, P., and Chapman, E. R. (2002) C2A activates a cryptic $Ca^{2+}$-triggered membrane penetration activity within the C2B domain of synaptotagmin I. *Proc. Natl. Acad. Sci. U. S. A. 99*, 1665−1670.
(29) Hui, E., Bai, J., and Chapman, E. R. (2006) $Ca^{2+}$-triggered simultaneous membrane penetration of the tandem C2-domains of synaptotagmin I. *Biophys. J. 91*, 1767−1777.
(30) Lai, A. L., Tamm, L. K., Ellena, J. F., and Cafiso, D. S. (2011) Synaptotagmin 1 modulates lipid acyl chain order in lipid bilayers by demixing phosphatidylserine. *J. Biol. Chem. 286*, 25291−25300.
(31) Herrick, D. Z., Kuo, W., Huang, H., Schwieters, C. D., Ellena, J. F., and Cafiso, D. S. (2009) Solution and membrane-bound conformations of the tandem C2A and C2B domains of synaptotagmin 1: evidence for bilayer bridging. *J. Mol. Biol. 390*, 913−923.
(32) Zhang, X., Rizo, J., and Sudhof, T. C. (1998) Mechanism of phospholipid binding by the C2A-domain of synaptotagmin I. *Biochemistry 37*, 12395−12403.
(33) Gerber, S. H., Rizo, J., and Sudhof, T. C. (2002) Role of electrostatic and hydrophobic interactions in $Ca^{2+}$-dependent phospholipid binding by the C2A-domain from synaptotagmin I. *Diabetes 51* (Suppl. 1), S12−S18.
(34) Sudhof, T. C. (2002) Synaptotagmins: why so many? *J. Biol. Chem. 277*, 7629−7632.
(35) Gauthier, B. R., Duhamel, D. L., Iezzi, M., Theander, S., Saltel, F., Fukuda, M., Wehrle-Haller, B., and Wollheim, C. B. (2007) Synaptotagmin VII splice variants alpha, beta, and delta are expressed in pancreatic beta-cells and regulate insulin exocytosis. *FASEB J. 22*, 194−206.
(36) Weir, G. C., and Bonner-Weir, S. (2004) Five stages of evolving beta-cell dysfunction during progression to diabetes. *Diabetes 53* (Suppl. 3), S16−S21.
(37) Brandt, D. S., Coffman, M. D., Falke, J. J., and Knight, J. D. (2012) Hydrophobic contributions to the membrane docking of synaptotagmin 7 C2A domain: mechanistic contrast between isoforms 1 and 7. *Biochemistry 51*, 7654−7664.
(38) Nalefski, E. A., Wisner, M. A., Chen, J. Z., Sprang, S. R., Fukuda, M., Mikoshiba, K., and Falke, J. J. (2001) C2 domains from different $Ca^{2+}$ signaling pathways display functional and mechanistic diversity. *Biochemistry 40*, 3089−3100.
(39) Ubach, J., Lao, Y., Fernandez, I., Arac, D., Sudhof, T. C., and Rizo, J. (2001) The C2B domain of synaptotagmin I is a $Ca^{2+}$-binding module. *Biochemistry 40*, 5854−5860.
(40) Maximov, A., Lao, Y., Li, H., Chen, X., Rizo, J., Sørensen, J. B., and Südhof, T. C. (2008) Genetic analysis of synaptotagmin-7 function in synaptic vesicle exocytosis. *Proc. Natl. Acad. Sci. U. S. A. 105*, 3986−3991.
(41) Landgraf, K. E., Malmberg, N. J., and Falke, J. J. (2008) Effect of $PIP_2$ binding on the membrane docking geometry of PKC$\alpha$ C2 domain: An EPR site-directed spin-labeling and relaxation study. *Biochemistry 47*, 8301−8316.
(42) Chen, H. C., Ziemba, B. P., Landgraf, K. E., Corbin, J. A., and Falke, J. J. (2012) Membrane docking geometry of GRP1 PH domain bound to a target lipid bilayer: an EPR site-directed spin-labeling and relaxation study. *PLoS One 7*, e33640.
(43) Hagelueken, G., Ward, R., Naismith, J. H., and Schiemann, O. (2012) MtsslWizard: in silico spin-labeling and generation of distance distributions in PyMOL. *Appl. Magn. Reson. 42*, 377−391.
(44) Stone, T. J., Buckman, T., Nordio, P. L., and McConnell, H. M. (1965) Spin-labeled biomolecules. *Proc. Natl. Acad. Sci. U. S. A. 54*, 1010−1017.
(45) Frazier, A. A., Wisner, M. A., Malmberg, N. J., Victor, K. G., Fanucci, G. E., Nalefski, E. A., Falke, J. J., and Cafiso, D. S. (2002) Membrane orientation and position of the C2 domain from $cPLA_2$ by site-directed spin labeling. *Biochemistry 41*, 6282−6292.
(46) Tombolato, F., Ferrarini, A., and Freed, J. H. (2006) Dynamics of the nitroxide side chain in spin-labeled proteins. *J. Phys. Chem. B 110*, 26248−26259.
(47) Shao, X., Fernandez, I., Sudhof, T. C., and Rizo, J. (1998) Solution structures of the $Ca^{2+}$-free and $Ca^{2+}$-bound C2A domain of synaptotagmin I: does $Ca^{2+}$ induce a conformational change? *Biochemistry 37*, 16106−16115.
(48) Malmberg, N. J., Van Buskirk, D. R., and Falke, J. J. (2003) Membrane-docking loops of the $cPLA_2$ C2 domain: detailed structural analysis of the protein-membrane interface via site-directed spin-labeling. *Biochemistry 42*, 13227−13240.
(49) Hui, E., Bai, J., Wang, P., Sugimori, M., Llinas, R. R., and Chapman, E. R. (2005) Three distinct kinetic groupings of the synaptotagmin family: candidate sensors for rapid and delayed exocytosis. *Proc. Natl. Acad. Sci. U. S. A. 102*, 5210−5214.
(50) Ellena, J. F., Lackowicz, P., Mongomery, H., and Cafiso, D. S. (2011) Membrane thickness varies around the circumference of the transmembrane protein BtuB. *Biophys. J. 100*, 1280−1287.


DOI: 10.1021/acs.biochem.5b00421
*Biochemistry* 2015, 54, 5684−5695